Design of Wide-Beam Leaky-Wave Antenna Arrays Based on the Bilinear Transformation of IIR Digital Filters and the *Z* Transform

Rafael Verdú-Monedero,* José-Luis Gómez-Tornero, and Juan Morales-Sánchez

In the pioneering work, the radiation diagrams of leaky wave antenna arrays can achieve attenuation nulls and gains at specific angles by manually placing the zeros and the poles in the *Z* domain of the corresponding discrete linear time-invariant (LTI) system. This handcrafted design procedure does not allow radiation diagrams with wide beams since the interaction between poles involved in the wide beam and their corresponding leaky modes cannot be easily handled. To overcome this limitation, this paper describes a novel method for designing radiation diagrams of leaky-wave antenna arrays based on the theory of IIR discrete filters. The proposed method relies on the design of discrete filters with the prototypes of analog low-pass filters defined by Butterworth and Chebyshev type I polynomials, whose roots along with the bilinear transformation provide the location of the poles and the zeros of the discrete LTI system and, therefore, the parameters of the leaky-wave antenna array. Results with different designs and a comparison with other approaches show the utility and effectiveness of this novel method to design wide-beam leaky-wave antenna arrays.

1. Introduction

Leaky-wave antennas (LWAs) are a class of antennas that use a traveling wave on a guiding structure as the main radiation mechanism.[1] LWAs offer a simpler topology, with a single feeding, which avoids the complex, bulky, and lossy beam forming networks associated with antenna arrays. LWAs possess interesting characteristics such as high gain, simple feeding network, and frequency scanning capability.[2] The radiation diagrams of LWA arrays can be designed by setting the leakage constant and

R. Verdú-Monedero, J.-L. Gómez-Tornero, J. Morales-Sánchez
Department of Tecnologías de la Información y las Comunicaciones
Universidad Politécnica de Cartagena
Cartagena 30202, Spain
E-mail: rafael.verdu@upct.es

phase constant along each antenna, providing single-beam beamforming with side lobe suppression, and generating multiple scanned beams or radiation nulls. This last feature is of special interest for modern multibeam and reconfigurable antennas operating in 5G and future 6G wireless networks.[3,4]

In the present paper, the efficient synthesis of broadbeam radiation patterns using LWAs is addressed. This type of confined patterns cover a wide angular region with stable gain and high rejection out of this prescribed zone, acting as an angular filter that allows robust reception of the radio signal in the prescribed angular region while rejecting the signals received out of this angular zone. The initial designs of wide-beam LWAs were based on single curved uniform LWAs[5] where the radiating angle is scanned due to the long-antenna curvature that covers the prescribed angular region, and later on single rectilinear LWAs, which were conveniently modulated[6–9] to create angular filter patterns.[10,11] This type of pattern is very beneficial due to its capability of interference mitigation and latency reduction in radiolinks,[12,13] improvement of robustness against direction-of-arrival (DoA) ambiguities in radars,[14] or increase the efficiency in wireless power transmission systems.[15,16]

In this context, the *Z* transform was proposed as a powerful tool in ref. [17] to synthesize designs of radiation patterns with nulls at prescribed angles using a phased-array of electronically reconfigurable LWAs. In that paper, this relationship between the illumination of such antennas and the impulse response of linear and time invariant (LTI) systems was provided. Using this perspective from the signal processing point of view, the exact locations of the poles and zeros of the *Z* transform of the associated *P*th order discrete LTI system provide all parameters of an array of *P* LWAs whose radiation pattern fulfills the specifications that have been initially prescribed (mainly the directions of the main lobes and their surrounding radiation nulls). Then, the positions of these poles and zeros in the *Z* plane can be converted into particular values of the LWA array control coefficients.

After this introduction, the rest of the paper is structured as follows: Section Method introduces the definition of an array of LWAs with its parameters and, by comparing the radiating-aperture illumination of an array of *P* LWAs and the spatial

impulse response of a discrete P-th order LTI system, establishes the correspondence between the poles and zeros of the discrete LTI system and the parameters of the array of P LWAs whose radiation pattern satisfies the desired requirements. After that, the proposed steps of the design procedure for providing the parameters of an array of antennas from a prescribed radiation diagram with wide beams are detailed. Section Results contains four wide-beam LWA arrays designed with this new method. The first two designs belong to a comprehensive example to describe thoroughly all the steps of the design procedure, whereas the last two designs are devoted to comparing the performance of the proposed method with the approach followed in ref. [18]. Finally, the last section closes the paper with the conclusions

2. Experimental Section

The radiating-aperture illumination function of an array with P semi-infinite LWAs is given by[1]

$$h(\gamma) = \sum_{i=1}^{P} D_i \, e^{-\alpha_i \gamma} \, e^{-j\beta_i \gamma} \, u(\gamma) \tag{1}$$

where D_i is a complex weight or excitation constant, α_i and β_i are, respectively, the leakage constant (nep m^{-1}) and the phase constant (rad m^{-1}) of the ith leaky mode, γ is the continuous spatial variable and $u(\gamma)$ is the Heaviside step signal, which is zero for the values $\gamma < 0$.

The elevation-plane radiation diagram of this antenna is given by the following expression[1]

$$H_R(\theta) = \int_{-\infty}^{\infty} h(\gamma) \, e^{jk_0 \sin(\theta)\gamma} d\gamma \tag{2}$$

where $\theta \in [-90°, \, 90°]$ is the elevation angle and the constant $k_0 = 2\pi/\lambda$ is the free-space wave number.

As described in ref. [17], the corresponding impulse response of the discrete Pth order LTI system could be computed by considering that $h(\gamma)$ is sampled using a spatial period (or spatial discretization step) Δ_γ,

$$h[n] = h(\gamma)|_{\gamma=n\Delta_\gamma} \tag{3}$$

and considering that the aperture of the antenna has a finite length L_A, that is, the illumination function is zero for values $\gamma < 0$ and for $\gamma > L_A$. Consequently, the discrete sequence obtained by this sampling is zero for values $n < 0$ and for $n > N_A$, where $N_A = \text{round}(L_A/\Delta_\gamma)$. This process of limiting the length of the illumination (Equation (3)) can be expressed as a spatial windowing

$$h_w[n] = h[n] \cdot w[n] \tag{4}$$

where $w[n]$ is a window with a length of N_A samples.

From the discrete sequence $h_w[n]$, its N-point discrete Fourier transform, DFT_N, can be calculated as

$$H_w[k] = \text{DFT}_N\{h_w[n]\} = \sum_{n=0}^{N-1} h_w[n] \, e^{-j\frac{2\pi}{N}kn} \tag{5}$$

with $k = 0, \ldots, N-1$ and $N \geq N_A$. As summarized in ref. [17], given the N-point discrete Fourier transform of the sequence $h_w[n]$, the radiation diagram $H_R(\theta)$ of a LWA can be computed at certain radiation angles θ_k since

$$\theta_k = \arcsin\left(-\frac{2\pi}{k_0 \Delta_\gamma N} k\right) \tag{6}$$

The other key result of ref. [17] was the relationship between the Z-transform of a P-order LTI system with P nonzero poles $p_i = r_{p_i} e^{j\omega_{p_i}}$

$$H_d^{P_P}(z) = \sum_{i=1}^{P} \frac{A_i}{1 - p_i z^{-1}} \tag{7}$$

whose causal impulse response in the spatial domain is

$$h^{P_P}[n] = \sum_{i=1}^{P} A_i p_i^n \, u[n] \tag{8}$$

and the discrete counterpart of the corresponding array of P LWAs with P leaky modes is

$$h^{L_P}[n] = \sum_{i=1}^{P} D_i \, e^{-\alpha_i \Delta_\gamma n} \, e^{-j\beta_i \Delta_\gamma n} \, u[n] \tag{9}$$

The aim of ref. [17] was to illustrate the new approach and the results were focused on showing the ability to design LWA arrays with nulls at desired angles. In those designs the systems were relatively simple, with a low order, and the poles and zeros were manually placed in the Z-plane. In the current paper, the radiation diagrams were required to have a wide-beam which could not be designed by manually placing the poles because the interference between them was not easy to control manually. To overcome this caveat, the design of radiation diagrams with wide beams would rely on the design of discrete low-pass filters and a subsequent modulation. Since the design of low-pass digital filters was based on classical methods for analog low-pass filters together with a frequency transformation, the bilinear transform was used in the proposed approach to transform continuous(-time) system representations to discrete(-time) and vice versa.

2.1. Design Procedure

Next, the steps of the proposed method to provide the parameters of a LWA from a set of specifications in the angular domain θ are described.

2.1.1. Specifications of the Radiation Diagram

In order to design radiation diagrams $H_R(\theta)$ with a wide beam, a template in the angular domain has to be defined (see **Figure 1**). This template is characterized by the set of parameters

$$[\theta_{P_1}, \, \theta_{P_2}, \, \Delta_\theta, \, \alpha_p, \, \alpha_a], \tag{10}$$

ADVANCED
SCIENCE NEWS
www.advancedsciencenews.com

ADVANCED
THEORY AND
SIMULATIONS
www.advtheorysimul.com
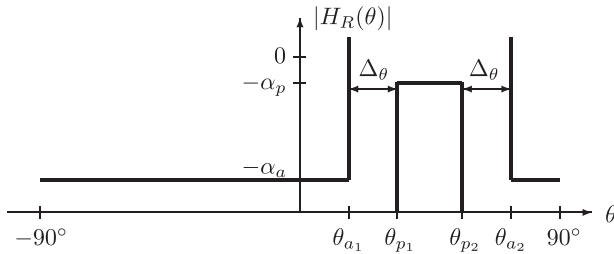
Figure 1. Template of specifications with parameters $[\theta_{p_1}, \theta_{p_2}, \Delta_\theta, \alpha_p, \alpha_a]$ for the radiation diagram $H_R(\theta)$ in the angular domain θ.

Figure 2. Template of specifications for the discrete band-pass system $H_{BP}(e^{j\omega})$ in the frequency domain ω.
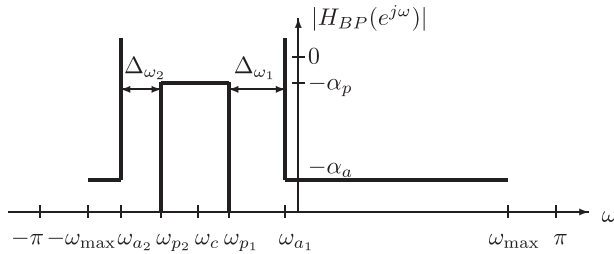
where θ_{p_1} is the lower angle of the beam, θ_{p_2} is the upper angle of the beam ($\theta_{p_2} > \theta_{p_1}$), Δ_θ is the maximum width of the transition band in the angular domain θ, α_p is the maximum relative attenuation in the radiated main wide beam (pass band) in dBs, and α_a is the minimum relative attenuation of the adjacent beams (stop band) in dBs. Other useful variables that can be obtained from these parameters are $\theta_{a_1} = \theta_{p_1} - \Delta_\theta$ and $\theta_{a_2} = \theta_{p_2} + \Delta_\theta$, which, as depicted in Figure 1, define the upper limit and the lower limit of the lower and upper stop bands, respectively.

2.1.2. Specifications of the Discrete LTI Band-Pass System

Using the relationship provided in ref. [17] between LWA arrays and the corresponding discrete LTI system, the frequency variable ω of the associated discrete LTI system is given by

$$\omega = -k_0 \Delta_\gamma \sin(\theta) \tag{11}$$

where Δ_γ is the spatial period (or spatial discretization step) used to sample the illumination $h(\gamma)$ in Equation (3). Considering the relationship given in Equation (11), the specifications in the angular domain θ are translated into the frequency domain ω (see **Figure 2**) of the corresponding discrete LTI system $H_{BP}(e^{j\omega})$. Please note the 2π-periodicity of $H_{BP}(e^{j\omega})$ as it is the Fourier transform of a discrete signal. The parameters that define the template of this band-pass system in the frequency domain ω are $\omega_{p_1} = -k_0 \Delta_\gamma \sin(\theta_{p_1})$ and $\omega_{p_2} = -k_0 \Delta_\gamma \sin(\theta_{p_2})$, which are, respectively, the upper and lower frequencies of the pass-band. The lower frequency of the upper stop-band is $\omega_{a_1} = -k_0 \Delta_\gamma \sin(\theta_{a_1})$ and the upper frequency of the lower stop-band is $\omega_{a_2} = -k_0 \Delta_\gamma \sin(\theta_{a_2})$. Generally, given the non linearity of Equation (11), the width of the transition bands are different, the maximum width of the upper transition band is $\Delta_{\omega_1} = \omega_{a_1} - \omega_{p_1}$ whereas the maximum width of the lower transition band is $\Delta_{\omega_2} = \omega_{p_2} - \omega_{a_2}$. The
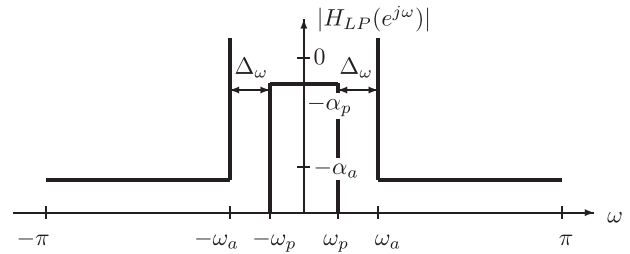
Figure 3. Template of specifications with parameters $[\omega_p, \omega_a, \alpha_p, \alpha_a]$ for the discrete low-pass system $H_{LP}(e^{j\omega})$ in the frequency domain ω.

limit of the visible margin in the θ domain is translated into the frequency domain as $\omega_{\max} = -k_0 \Delta_\gamma \sin(-90°) = k_0 \Delta_\gamma$. Another useful parameter is the central frequency of the pass band, which can be obtained as $\omega_c = (\omega_{p_1} + \omega_{p_2})/2$.

2.1.3. Specifications of the Discrete LTI Low-Pass System

The techniques for designing digital filters need specifications of a low-pass system. Then, the system $H_{LP}(e^{j\omega})$ is defined as

$$H_{LP}(e^{j\omega}) = H_{BP}(e^{j(\omega+\omega_c)}) \tag{12}$$

As depicted in **Figure 3**, the 2π-periodic template with specifications of the low-pass system $H_{LP}(e^{j\omega})$ is defined by the set

$$[\omega_p, \omega_a, \alpha_p, \alpha_a] \tag{13}$$

where $\omega_p = \omega_{p_1} - \omega_c = (\omega_{p_1} - \omega_{p_2})/2$ is the maximum frequency of the pass-band, $\omega_a = \omega_p + \Delta_\omega$ is the minimum frequency of the stop-band, with $\Delta_\omega = \min\{\Delta_{\omega_1}, \Delta_{\omega_2}\}$ being the width of the transition band.

2.1.4. Specifications of the Continuous LTI Low-Pass System

The design of a discrete low-pass filter usually relies on analog prototypes using a transformation which maps the s-plane poles and zeros of the analogue filter into the z plane. In the proposed approach, the specifications of the analog low-pass prototype $H(j\Omega)$ were obtained by using the bilinear transformation, which did not produce aliasing as the impulse invariance method.[19] The bilinear transformation mapped one revolution of the unit circle in the z-plane to the entire $j\Omega$-axis in the s-plane[20]

$$\Omega = \frac{2}{T_d} \tan\left(\frac{\omega}{2}\right) \tag{14}$$

where T_d is the discretization step which relates the spatial counterparts of $H_{LP}(e^{j\omega})$ and $H(j\Omega)$.[20] This nonlinear transformation maps $-\infty \leq \Omega \leq \infty$ onto $-\pi \leq \omega \leq \pi$ (see **Figure 4**). The template of the analog filter is characterized by the set of parameters

$$[\Omega_p, \Omega_a, \alpha_p, \alpha_a] \tag{15}$$

where $\Omega_p = \frac{2}{T_d} \tan(\frac{\omega_p}{2})$ is the maximum frequency of the pass-band and $\Omega_a = \frac{2}{T_d} \tan(\frac{\omega_a}{2})$ is the minimum frequency of the

**ADVANCED
SCIENCE NEWS**

www.advancedsciencenews.com

**ADVANCED
THEORY AND
SIMULATIONS**

www.advtheorysimul.com
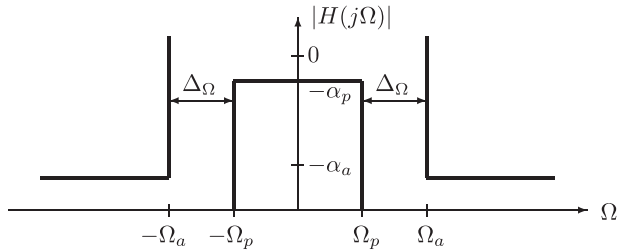
Figure 4. Template of specifications with parameters $[\Omega_p, \Omega_a, \alpha_p, \alpha_a]$ for the analog low-pass system $H(j\Omega)$ in the frequency domain Ω.

stop-band. The values α_p and α_a did not suffer any transformation and kept the same values as those of the LWA array in Equation (10) since the amplitude was normalized.

2.1.5. Design of the Analog Low-Pass Filter

With the specifications defined in Equation (15), a continuous low-pass filter $H(s)$ is designed,

$$H(j\Omega) = H(s)|_{s=j\Omega} \tag{16}$$

This Pth order analog prototype was built with Butterworth or Chebyshev type I polynomials (Chebyshev type II or elliptic polynomials were discarded since they usually provide a discontinuity of the spatial response at the origin which could not be synthesized by an LWA array).

2.1.6. Obtaining the Discrete Low-Pass Filter

Undoing the bilinear transformation, the low-pass discrete system is given by

$$H_{LP}(z) = H(s)\Big|_{s=\frac{2}{T_d}\frac{1-z^{-1}}{1+z^{-1}}} \tag{17}$$

2.1.7. Obtaining the Discrete Band-Pass Filter

The band-pass system could be obtained from the low-pass system considering the shifting in the frequency domain (Equation (12)), then

$$H_{BP}(z) = H_{LP}\left(z \cdot e^{-j\omega_c}\right) \tag{18}$$

As expressed in Equation (12), the counterpart of previous equation in the spatial domain established that $h_{BP}[n]$ could be understood as a modulation of $h_{LP}[n]$, that is,

$$h_{BP}[n] = h_{LP}[n] \cdot e^{j\omega_c n} \tag{19}$$

Finally, since the antenna was not infinite, a windowing in the spatial domain had to be considered

$$h_{BP}^w[n] = h_{BP}[n]\, w[n] \tag{20}$$

2.1.8. Obtaining the Parameters of the LWA Array

Considering the P nonzero poles $p_i = r_{p_i} e^{j\omega_{p_i}}$ and expressing the band-pass system by its partial fraction decomposition, that is,

$$H_{BP}(z) = \sum_{i=1}^{P} \frac{A_i}{1 - p_i z^{-1}} \tag{21}$$

the parameters of the leaky modes of the LWA array were determined by the zeros and poles of the corresponding LTI system[17]

$$\alpha_i = -\frac{\ln(r_{p_i})}{\Delta_\gamma} \tag{22}$$

$$\beta_i = -\frac{\omega_{p_i}}{\Delta_\gamma} \tag{23}$$

$$D_i = A_i \tag{24}$$

Therefore, an LWA array with P leaky modes is equivalent to a Pth order discrete LTI system in which the amplitude and the phase of each pole p_i determine the leakage and phase constants of each leaky mode, α_i and β_i, respectively, and each residue A_i gives the associated coefficient D_i, according to Equations (22)–(24).

3. Results

In the following experiments, the antennas work at a frequency of $f = 15$ GHz (with the corresponding wavelength in the free space $\lambda_0 = 0.02$ m and wavenumber in the free space $k_0 = 314.1593$ rad m^{-1}). To ensure that no aliasing affects the reconstruction of the continuous illumination $h(\gamma)$ from its discrete counterpart $h[n]$, the spatial discretization step is set to $\Delta_\gamma = \lambda_0/10 = 2 \times 10^{-3}$ m (which is smaller than $\lambda_0/2$[21,22]). The length of the antenna is $L_A = 20 \times \lambda_0 = 0.40$ m in Design #1 and Design #2, and $L_A = 7.5 \times \lambda_0 = 0.15$ m in Design #3 and Design #4, which provides the length of the discrete signals of $N_A = 200$ and $N_A = 75$ samples, respectively. The amplitudes of these finite-length discrete signals have not been further modified since a rectangular window $w[n]$ has been used in Equation (20). The size of the FFT's is $N = 2^{16}$ points, which fulfills more than enough of the condition $N > N_A$.[20]

3.1. Comprehensive Example

The first results are devoted to explain carefully the proposed steps for designing an array of LWAs given a template with the set of specifications. The steps followed are those detailed in Experimental Section (Design Procedure) and depicted in **Figure 5**. Initially, the values of the parameters that make up the template of specifications in the angular domain (Equation (10)) are established:

$$\begin{bmatrix} \theta_{P_1}, & \theta_{P_2}, & \Delta_\theta, & \alpha_p, & \alpha_a \end{bmatrix} = \begin{bmatrix} 10°, & 40°, & 10°, & 1\,dB, & 20\,dB \end{bmatrix}$$

**ADVANCED
SCIENCE NEWS**

www.advancedsciencenews.com

**ADVANCED
THEORY AND
SIMULATIONS**

www.advtheorysimul.com

1. Specifications of the radiation diagram

Beam width $\qquad \rightarrow \theta_{p_1}, \theta_{p_2}$

Transition band $\qquad \rightarrow \Delta_\theta$

Atenuations $\qquad \rightarrow \alpha_p, \alpha_a$

2. Specifications of the discrete band-pass system

$\omega = -k_0 \Delta_y \sin(\theta) \qquad \rightarrow [\omega_{p_1}, \omega_{p_2}, \omega_{a_1}, \omega_{a_2}]$
$\qquad\qquad\qquad\qquad \rightarrow [\Delta_{\omega_1}, \Delta_{\omega_2}, \omega_c]$

3. Specifications of the discrete low-pass system

$\omega_{LP} = \omega_{BP} + \omega_c \qquad \rightarrow [\omega_p, \omega_a, \alpha_p, \alpha_a]$

4. Specifications of the analog low-pass system

$\Omega = \frac{2}{T_d} \tan\left(\frac{\omega}{2}\right) \qquad \rightarrow [\Omega_p, \Omega_a, \alpha_p, \alpha_a]$

5. Design of analog low-pass filter

$[\Omega_p, \Omega_a, \alpha_p, \alpha_a]$ and filter type $\qquad \rightarrow H(s)$

6. Obtaining the discrete low-pass filter

$H_{LP}(z) = H(s)\Big|_{s = \frac{2}{T_d} \frac{1-z^{-1}}{1+z^{-1}}}$

7. Obtaining the discrete band-pass filter

$H_{BP}(z) = H_{LP}\left(z \cdot e^{-j\omega_c}\right)$
$H_{BP}(z) = \sum_{i=1}^{P} \frac{A_i}{1 - p_i z^{-1}}, \quad \text{with } p_i = r_{p_i} e^{j\omega_{p_i}}$

8. Parameters of the LWA array

$\alpha_i = -\ln(r_{p_i})/\Delta_y$
$\beta_i = -\omega_{p_i}/\Delta_y$
$D_i = A_i$ (residues of partial frac. exp.)

Figure 5. Workflow of the proposed approach to design LWA arrays with wide beams by means of a discrete LTI band-pass system.

Next, previous specifications are translated into the frequency domain ω of the discrete band-pass system by the relationship given in Equation (11), providing: $\omega_{p_1} = -0.1091$, $\omega_{p_2} = -0.4039$, $\omega_{a_1} = 0.0000$, $\omega_{a_2} = -0.4813$, the central frequency of the pass band $\omega_c = -0.2565$ and the maximum width of the transition band $\Delta_\omega = 0.0774$. Taking into account these values and Equation (12), the template of specifications (Equation (13)) of the discrete low-pass system is

$$[\quad \omega_p, \quad \omega_a, \quad \alpha_p, \quad \alpha_a \quad] =$$
$$[\quad 0.1474, \quad 0.2248, \quad 1\,\text{dB}, \quad 20\,\text{dB} \quad]$$

Considering the bilinear transformation (Equation (14)) with $T_d = \Delta_y$, the template of specifications of the analog low-pass filter (Equation (15)) is given by

$$[\quad \Omega_p, \quad \Omega_a, \quad \alpha_p, \quad \alpha_a \quad] =$$
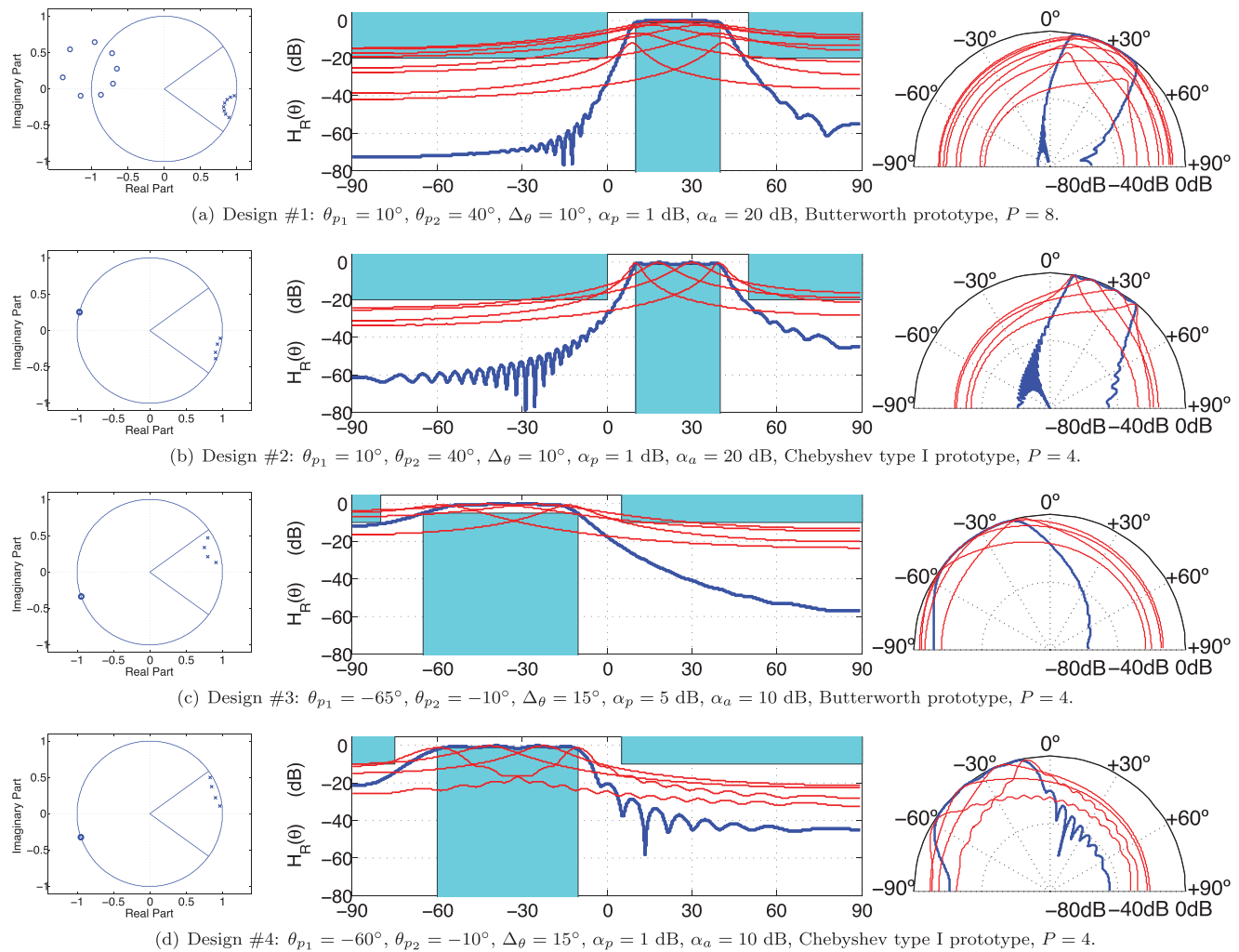$$[\quad 73.8259\,\text{rad}, \quad 112.8905\,\text{rad}, \quad 1\,\text{dB}, \quad 20\,\text{dB} \quad]$$

In Design #1, choosing a Butterworth prototype, the analog low-pass filter obtained that fulfills previous requirements has order $P = 8$, whereas in Design #2, if a Chebyshev type I prototype is used instead, the order is $P = 4$. As can be observed, the designs based on Chebyshev polynomials need a lower order than those based on Butterworth polynomials at the cost of the existence of ripple in the passband. The corresponding discrete low-pass filter $H_{LP}(z)$ is derived from the analog prototype $H(s)$ using Equation (17), and the relationship between the s domain of the analog low-pass filter and the z domain of the discrete low-pass filter is

$$z = \frac{1 + \frac{T_d}{2} s}{1 - \frac{T_d}{2} s} \tag{25}$$

Finally, the discrete band-pass filter $H_{BP}(z)$ is obtained from previous low-pass filter $H_{LP}(z)$ by a circular concentric shift in the z-domain (see Equation (18)). The poles p_i of $H_{BP}(z)$ are related to the poles s_i of the analog prototype $H(s)$ by the expression

$$p_i = \frac{1 + \frac{T_d}{2} s_i}{1 - \frac{T_d}{2} s_i} \cdot e^{-j\omega_c} \tag{26}$$

Table 2 gathers in detail the poles and zeros of $H_{BP}(z)$ in Design #1 and Design #2 as well as the corresponding parameters of the LWA array. As stated in Equation (21), each pole p_i of $H_{BP}(z)$ provides the parameters α_i and β_i of each one of the leaky modes that compose the LWA array (see Equations (22) and (23)) whereas the zeros are related with the coefficients A_i and therefore with D_i (see Equation (24)). The zero–pole plot of these two designs can be seen on the left part of the two first rows in **Figure 6**. The central column of this figure shows the radiation diagram $H_R(\theta)$ of the LWA array in blue color and each one of its leaky modes are plotted in red color. Note how the response of the LWA array can achieve higher attenuation than an isolate leaky mode thanks to the interference produced between the modes. Since the location of the poles and zeros is given, in the proposed method, by the roots of the Butterworth or Chebyshev type I polynomials, it is possible to design radiation diagrams $H_R(\theta)$ with wide beams and

**ADVANCED
SCIENCE NEWS**

www.advancedsciencenews.com

**ADVANCED
THEORY AND
SIMULATIONS**

www.advtheorysimul.com

(a) Design #1: $\theta_{p_1} = 10°$, $\theta_{p_2} = 40°$, $\Delta_\theta = 10°$, $\alpha_p = 1$ dB, $\alpha_a = 20$ dB, Butterworth prototype, $P = 8$.

(b) Design #2: $\theta_{p_1} = 10°$, $\theta_{p_2} = 40°$, $\Delta_\theta = 10°$, $\alpha_p = 1$ dB, $\alpha_a = 20$ dB, Chebyshev type I prototype, $P = 4$.

(c) Design #3: $\theta_{p_1} = -65°$, $\theta_{p_2} = -10°$, $\Delta_\theta = 15°$, $\alpha_p = 5$ dB, $\alpha_a = 10$ dB, Butterworth prototype, $P = 4$.

(d) Design #4: $\theta_{p_1} = -60°$, $\theta_{p_2} = -10°$, $\Delta_\theta = 15°$, $\alpha_p = 1$ dB, $\alpha_a = 10$ dB, Chebyshev type I prototype, $P = 4$.

Figure 6. Designs of LWA arrays based on discrete LTI pass-band filters. First column shows the zero–pole plots of the corresponding discrete LTI pass-band system, the second column contains the radiation diagram of each LWA array in blue color as well as the response of each leaky mode that forms the array in red color. The specifications are depicted with the light blue template. The third column shows the radiation diagrams in polar coordinates. Details of the experiments are gathered in Tables 1 and 2.

high attenuation which can not be obtained by placing manually these roots in the z plane (as described in ref. [17]) since the interference between the modes can not been easily handled when the order P increases. The plots on the right part of these two rows in Figure 6 show the radiation diagram in polar coordinates of the LWA array and the radiation diagram of each mode that makes up the array. In Figure 6b the ripple in the pass-band produced by Chebyshev polynomials can be noticed, however, the resulting radiation diagram accomplishes the set of specifications (plotted in the template in light blue).

3.2. Comparative Design

In order to evaluate the performance of the proposed approach, the radiation diagram addressed in ref. [18] is going to be compared with two designs obtained with the proposed method. To make a fair comparison, the designs provided by the proposed

method will be limited to fourth order ($P = 4$), as the LWA array used in ref. [18]. As the order P of the spatial filter increases, the rejection can be enhanced. However, this also increases the number of elements of the antenna array, which translates in a larger antenna and a more complex distribution network to feed the P elements of the array. For this reason, the synthesis of broadbeam patterns with LWA arrays usually have a low value of P, such as $P = 2$[23] or $P = 3$.[18] Also, as the order P increases, the synthesis of the broadbeam created by the interference of P scanned beams becomes more complicated, thus making necessary iterative optimization methods such as in refs. [24, 25], or even relying on deep learning approaches as proposed in ref. [26]. Our synthesis method is direct, and can provide the array weighting coefficients for any value of P, as demonstrated in ref. [27] for $P = 11$.

To demonstrate the usefulness of the proposed method, we compare with the design in ref. [18] using $P = 4$, which was optimized using a trial-and-error technique. As it will be shown,

ADVANCED
SCIENCE NEWS

www.advancedsciencenews.com

ADVANCED
THEORY AND
SIMULATIONS

www.advtheorysimul.com

Table 1. Specifications of the radiation diagram in the designs obtained with the proposed method.

Design number #	θ_{p_1}	θ_{p_2}	Δ_θ	α_p	α_a	Analog prototype
#1	10°	40°	10°	1 dB	20 dB	Butterworth
#2	10°	40°	10°	1 dB	20 dB	Chebyshev type I
#3	−65°	−10°	15°	5 dB	10 dB	Butterworth
#4	−60°	−10°	15°	1 dB	10 dB	Chebyshev type I

our method provides better synthesis in a direct way, without the need of iterative optimization.

Two designs have been developed with the proposed method, one of them based on a Butterworth prototype (Design #3) and the other based on a Chebyshev Type I prototype (Design #4). The set of specifications of these two designs are detailed in **Table 1**. The LWA array proposed in ref. [18] produces a broad beamwidth using an array of four LWAs in slotted substrate integrated waveguide (SIW) technology.

The four beam directions in ref. [18] were optimized with a trial-and-error procedure, in order to synthesize a broadbeam pattern covering the desired angular zone from −60° to −15°, while providing the higher rejection out of it. Table 3 summarizes the optimized scanning directions for each one of the four beams. The leakage rates of each beam, and their complex weighting coefficients were not optimized. Actually, the LWA array design in ref. [18] uses a four-way power divider with equal outputs of phase and amplitude. As a result, the weighting coefficients in Table 3 shows equal unity amplitudes and zero phases for the four com-

plex coefficients D_i. The proposed approach, directly provides the four beams directions from β_i/k_0, leakage rates α_i/k_0, and complex feeding coefficients D_i of each LWA, to synthesize a broad beam with certain specifications.
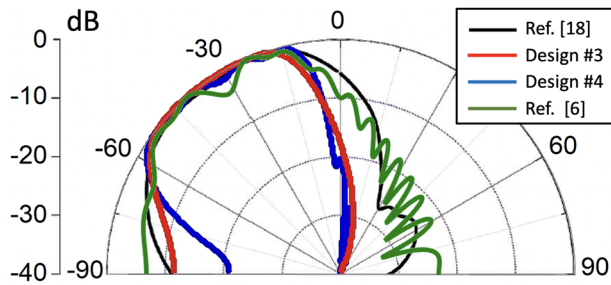
To prove the superior performance when compared to ref. [18], two radiation patterns are synthesized with the specifications summarized in Table 1, namely Design #3 and Design #4. Both designs have similar beam widths from $\theta_{p_1} = -65°$ to $\theta_{p_2} = -10°$ and similar transition band $\Delta_\theta = 15°$. However, Design #3 uses a Butterworth filter with attenuation $\alpha_p = 5$ dB and $\alpha_a = 10$ dB, while Design #4 uses a Chebyshev type I filter with $\alpha_p = 1$ dB and $\alpha_a = 10$ dB.

Third row and fourth row of Figure 6 show, respectively, the zero-pole plots of Design #3 and Design #4 provided by the proposed method, along with the resulting radiation diagrams. Third row and fourth row of **Table 2** detail the zeros and poles of the discrete LTI band-pass system, as well as the parameters α_i, β_i, and D_i of the LWA arrays for these two designs.

To compare our synthesis method with trial-and-error method in ref. [18], **Figure 7** shows the three radiation diagrams under comparison: Design #3 based on Butterworth prototype in red color, Design #4 based on Chebyshev type I prototype in blue color and the design described in ref. [18] in black color. As commented, the design proposed in ref. [18] is based on a manual superposition of $P = 4$ beams, which are assumed to have similar amplitude and phases. As a result, the beam directions are adjusted after a trial-and-error procedure which optimizes the overall interference pattern. Since the four beams produce complex radiated fields, the control on their relative amplitudes

Table 2. Parameters of the LTI systems and the corresponding leaky-wave antenna arrays.

Design number #	System order P	Poles			Zeros			Leaky wave antenna array parameters			
		Z plane		$H_R(\theta)$	Z plane		$H_R(\theta)$				
		r_{p_i}	ω_{p_i}	θ_{p_i}	r_{c_i}	ω_{c_i}	θ_{c_i}	α_i [nep m^{-1}]	β_i [rad m^{-1}]	D_i	L_A
#1	8	0.9693	−0.4138	41.1895°	1.4743	2.8851	-	15.5764	206.8900	0.0469 + 0.0315i	20 λ_0
		0.9693	−0.0992	9.0841°	1.3142	−3.1254	-	15.5764	49.6008	0.0469 − 0.0315i	
		0.9149	−0.1228	11.2741°	1.3142	2.6124	-	44.4604	61.4192	0.0572 + 0.2791i	
		0.9149	−0.3901	38.3842°	1.0063	−3.0119	-	44.4604	195.0716	0.0572 − 0.2791i	
		0.8750	−0.3461	33.4232°	1.0063	2.4989	-	66.7588	173.0448	−0.6786 + 0.1308i	
		0.8750	−0.1669	15.4036°	0.7613	−3.1123	-	66.7588	83.4461	−0.6786 − 0.1308i	
		0.8540	−0.2880	27.2846°	0.6690	2.8851	-	78.9319	144.0139	0.5745 + 0.8645i	
		0.8540	−0.2250	20.9790°	0.7613	2.5993	-	78.9319	112.4770	0.5745 − 0.8645i	
#2	4	0.9797	−0.1115	10.2247°	0.9966	2.8885	-	10.2477	55.7661	−0.0097 + 0.0191i	20 λ_0
		0.9797	−0.4014	39.7118°	1.0034	2.8885	-	10.2477	200.7248	−0.0097 − 0.0191i	
		0.9515	−0.3167	30.2629°	0.9966	2.8817	-	24.8524	158.3264	0.0097 + 0.0511i	
		0.9515	−0.1963	18.2080°	1.0034	2.8817	-	24.8524	98.1645	0.0097 − 0.0511i	
#3	4	0.9235	0.1456	−13.3997°	0.9973	−2.8050	-	39.8179	−72.8043	−0.0959 − 0.0406i	7.5 λ_0
		0.9235	0.5329	−58.0178°	1.0027	−2.8050	-	39.8179	−266.4739	−0.0959 + 0.0406i	
		0.8234	0.4203	−41.9892°	0.9973	−2.7996	-	97.1298	−210.1695	0.0959 − 0.2367i	
		0.8234	0.2582	−24.2655°	1.0027	−2.7996	-	97.1298	−129.1087	0.0959 + 0.2367i	
#4	4	0.9703	0.1126	−10.3278°	1.0000	−2.8099	-	15.0633	−56.3226	−0.0142 − 0.0281i	7.5 λ_0
		0.9703	0.5406	−59.3608°	0.9949	−2.8150	-	15.0633	−270.3005	−0.0142 + 0.0281i	
		0.9292	0.4156	−41.4148°	1.0000	−2.8200	-	36.7263	−207.8182	0.0142 − 0.0756i	
		0.9292	0.2376	−22.2202°	1.0051	−2.8150	-	36.7263	−118.8049	0.0142 + 0.0756i	

**ADVANCED
SCIENCE NEWS**

www.advancedsciencenews.com

**ADVANCED
THEORY AND
SIMULATIONS**

www.advtheorysimul.com

Figure 7. Comparison of results using the proposed approach with the result provided in ref. [18]. The radiation diagram $H_R(\theta)$ of Design #3 using a Butterworth analog prototype is plotted in red color, Design #4 using a Chebyshev type I analog prototype is plot in blue color, and the radiation diagram provided in ref. [18] is plotted in black color. In the three cases, the LWA array has $P = 4$ leaky modes and the LWAs length is $L_A = 7.5\lambda_0$. Also, the result for a single LWA of the same length $L_A = 7.5\lambda_0$ and modulated following the technique proposed in ref. [6] is plotted in green line.

Table 3. Comparative analysis of the parameters used by ref. [18] and the proposed approach.

Design number #	$\angle(\frac{\beta_i}{k_0})$	$\frac{\alpha_i}{k_0}$	$\frac{D_i}{D\text{max}}$	$\angle D_i$
#3	−13.3997°	0.1267	0.4078	−157.0570°
	−58.0178°	0.1267	0.4078	157.0570°
	−41.9892°	0.3092	1.0000	−67.9499°
	−24.2655°	0.3092	1.0000	67.9499°
#4	−10.3278°	0.0479	0.4098	−116.8002°
	−59.3608°	0.0479	0.4098	116.8002°
	−41.4148°	0.1169	1.0000	−79.3538°
	−22.2202°	0.1169	1.0000	79.3538°
[18]	−66°	-	1.0000	0.0000°
	−44°	-	1.0000	0.0000°
	−26°	-	1.0000	0.0000°
	−11°	-	1.0000	0.0000°

and phases can be essential to define the total interference pattern. As the number of overlapping beams P increases (higher order P) and/or the length of the LWA becomes larger, the manual synthesis is likely to be more complicated by diffraction and interference effects between beams. This can cause uncontrollable in-band ripple level and low attenuation in the rejection band, unsuitable for demanding spatial filtering specifications. On the other hand, the designs obtained with the proposed method are able to synthesize radiation diagrams with predetermined ripple and rejection levels as well as accurate angular precision.

This is demonstrated in Figure 7, where it can be observed how the designs obtained with the filter synthesis method provide higher rejection out of the prescribed passband angular region from −60° to −15°. Particularly, both Butterworth and Chebyshev spatial filter designs provide a rejection of −20 dB for $\theta = 0°$, while the design in ref. [18] shows a rejection of −5 dB. For the lower out-of-band zone at $\theta = -75°$, the design in ref. [18] shows similar rejection of −5 dB, while Design #3 based on Butterworth polynomial improves the rejection level to −10 dB, and Design #4 based on Chebyshev polynomial increases the rejection up to −20 dB. As expected, the Chebyshev synthesis provides higher rejection level, at the expense of an in-band ripple of 1 dB, which can also be observed in Figure 7. Also, the results obtained using the modulated angle technique proposed in ref. [6] are plotted in Figure 7, for a similar LWA length $L_A = 7.5\lambda_0$. This technique produces lower out-of-band rejection and higher ripple level, thus requesting further numerical optimization to shape the broad beam.[7] On the contrary, the technique proposed in this paper directly provides the requested angular filter specifications. In any case, the angular selectivity is higher than using a single modulated leaky wave,[27] due to the use of multiple leaky waves in parallel (in this case $P = 4$).

Figure 8 shows a in depth comparison between the LWA arrays provided by the proposed method using as analog prototype a Butterworth polynomial or a Chebyshev type I polynomial. As commented, the radiation patterns in Figure 8 show that the most selective but rippled response are given by the Chebyshev prototype. This is due to the fact that their leaky modes use a lower α/k_0 (see **Table 3**) and therefore illuminate the antenna aperture more efficiently. From the electromagnetic point of view, this fact
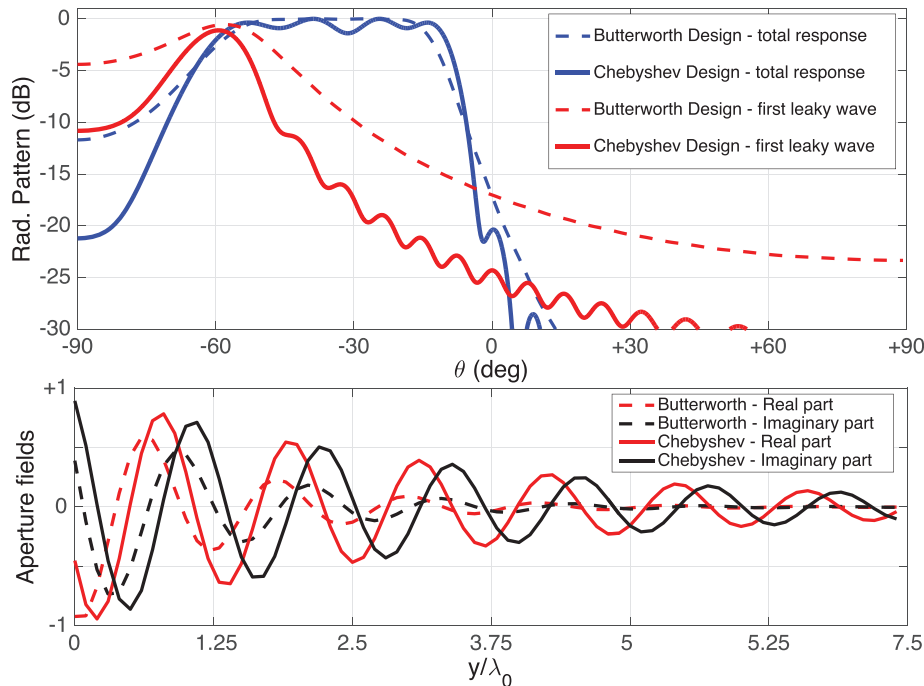
can be understood not only as a greater effective length of radiation but a greater diffraction at the edges of the antenna, resulting in a more directive radiation diagram but with larger secondary lobes. This is illustrated in the upper part of Figure 8 by showing the radiation pattern of one of the four beams (the one pointing at a lower angle $\theta = -60°$) for both Butterworth and Chebyshev designs. It is shown that the Chebyshev beams are more directive, and this creates narrower beams with higher rejection out of the scanning angle, but with higher ripple level associated to the secondary lobes. The lower part of Figure 8 illustrates the spatial illumination associated to this beam for the two designs. It can be clearly seen that the Chebyshev type I leaky wave with lower attenuation rate $\alpha/k_0 = 0.0479$ extends in the entire aperture, while the leaky wave of the Butterworth design with higher attenuation rate $\alpha/k_0 = 0.1267$ barely reaches the middle of the antenna. As a result, it can be concluded that Butterworth synthesis makes use of wider interference beams, while Chebyshev synthesis uses more directive beams. In any case, our direct synthesis method provides the exact beam direction and complex excitation coefficients for each LWA element, so that the interference pattern creates a broad beam with prescribed ripple and rejection specifications. As can be seen in Table 3, the complex weighting coefficients D_i are not uniform as assumed in ref. [18], but their amplitudes and phases are directly obtained, together with the beam direction and leakage rate for each one of the four elements of the LWA array.

Also, the proposed method can be extended for the synthesis of cosecant-squared radiation patterns. For that, the weighting coefficients D_i obtained for a flat-topped response can be later multiplied by the desired cosecant-squared power profile. This two-step technique has also been proposed in ref. [28] for the synthesis of cosecant-squared patterns using a single modulated LWA. Our initial results show that this method can similarly be applied for an array of LWAs, obtaining better performance using Chebyshev Type I polynomials than with Butterworth prototypes. However, as also stated in ref. [28], this technique normally needs further numerical optimization to reduce the ripple and sidelobe levels. In any case, this is out of the scope of the present

**ADVANCED
SCIENCE NEWS**

www.advancedsciencenews.com

**ADVANCED
THEORY AND
SIMULATIONS**

www.advtheorysimul.com

Figure 8. In depth comparison between Design #3 based on a Butterworth analog prototype and Design #4 based on a Chebyshev type I analog prototype. a) Radiation diagram of the total response $H_R(\theta)$ (in dashed blue line for the Butterworth design and in solid blue line for the Chebyshev design) and radiation diagram of only the first leaky mode (in dashed red line for the Butterworth design and in solid red line for the Chebyshev design). b) Spatial response (aperture fields) of the first leaky mode (real and imaginary part) for Design #3 and Design #4.

work, which is focused on the synthesis of flat-topped radiation patterns following pure Butterworth and Chebyshev type I angular responses.

4. Conclusions

This paper has shown a new method for designing wide-beam LWA arrays. This novel approach is based on the relationship between the zeros and poles of a discrete LTI low pass filter designed using Butterworth and Chebyshev type I polynomials and the parameters of an LWA array. The proposed method is able to produce a pass-band without ripple (using the Butterworth prototype), joint control on the pass-band and rejection band as well as a higher attenuation level in the rejection band than other techniques which assume that all the elements of the LWA array are fed with uniform amplitude and phase feeding coefficients. As it has been demonstrated, the proposed synthesis method directly provides the parameters of each LWA forming the array, namely the scanning direction, the leakage rate, and the complex feeding coefficient. Since each LWA creates a directive scanned beam, the manual location of each beam can lead to the synthesis of a broad beam with poorer performance, as demonstrated by comparing with previous works. This fact is more remarkable as the number of elements and/or the LWA length is higher.[28]

Conflict of Interest

The authors declare no conflict of interest.

Data Availability Statement

The paper describes a theoretical procedure, which is completely described and detailed in the paper.

[1] A. Oliner, D. Jackson, in *Antenna Engineering Handbook*, 4th ed., McGraw-Hill Education, New York, NY **2007**, Ch. 11, pp. 1–55.

[2] D. R. Jackson, C. Caloz, T. Itoh, *Proc. IEEE* **2012**, *100*, 2194.

[3] J. L. Gómez-Tornero, in *Antenna and Array Technologies for Future Wireless Ecosystems*, (Eds: Y. J. Guo, R. W. Ziolkowski), John Wiley & Sons, Hoboken, NJ **2022**, Ch. 4, pp. 119–181.

[4] K. Shen, W. Yu, *IEEE Trans. Signal Process.* **2018**, *66*, 2616.

[5] I. Ohtera, *IEEE Trans. Antennas Propag.* **1999**, *47*, 1470.

[6] P. Burghignoli, F. Frezza, A. Galli, G. Schettini, *IEEE Antennas Wireless Propag. Lett.* **2003**, *2*, 136.

[7] J. L. Gomez-Tornero, A. R. Weily, Y. J. Guo, *IEEE Trans. Antennas Propag.* **2011**, *59*, 3999.

[8] A. J. Martínez-Ros, J. L. Gómez-Tornero, G. Goussetis, *IEEE Trans. Antennas Propag.* **2013**, *61*, 3466.

[9] S. Khaefi, A. Mallahzadeh, M. H. Amini, *Opt. Commun.* **2021**, *485*, 126737.

[10] A. J. Martínez-Ros, J. L. Gómez-Tornero, G. Goussetis, *IEEE Antennas Wireless Propag. Lett.* **2017**, *16*, 936.

[11] C. Yepes, E. Gandini, S. Monni, A. Neto, F. E. van Vliet, D. Cavallo, *IEEE Antennas Wireless Propag. Lett.* **2020**, *19*, 408.

[12] Y. Geng, J. Wang, Z. Li, Y. Li, M. Chen, Z. Zhang, *IEEE Access* **2019**, *7*, 86367.

[13] F. M. Monavar, S. Shamsinejad, R. Mirzavand, J. Melzer, P. Mousavi, *IEEE Trans. Antennas Propag.* **2017**, *65*, 1108.

[14] M. Poveda-García, J. L. Gómez-Tornero, *IEEE Antennas Wireless Propag. Lett.* **2021**, *20*, 503.

[15] C. Chen, B. Zhang, K. Huang, *IEEE Antennas Wireless Propag. Lett.* **2019**, *18*, 1863.

[16] C. K. Wang, B. J. Xiang, S. Y. Zheng, K. W. Leung, W. S. Chan, Y. A. Liu, *IEEE Trans. Ind. Electron.* **2021**, *68*, 10709.

[17] R. Verdú-Monedero, J. Gómez-Tornero, *IEEE Trans. Signal Process.* **2019**, *67*, 2275.

[18] Y. Geng, J. Wang, in *2016 11th Int. Symp. on Antennas, Propagation and EM Theory (ISAPE)*, IEEE, Piscataway, NJ **2016**, pp. 159–162.

[19] L. B. Jackson, *Digital-Filter Implementation*, Springer US, Boston, MA **1996**, pp. 427–449.

[20] A. Oppenheim, R. Schafer, *Discrete-Time Signal Processing*, 3rd ed., Pearson, London **2010**.

[21] R. Elliott, *IEEE Trans. Antennas Propag.* **1977**, *25*, 617.

[22] R. E. Hodges, Y. Rahmat-Samii, *IEEE Trans. Antennas Propag.* **1996**, *44*, 1499.

[23] Y. Geng, J. Wang, Y. Li, Z. Li, M. Chen, Z. Zhang, *IEEE Trans. Antennas Propag.* **2018**, *66*, 6334.

[24] J. L. Gómez-Tornero, A. J. Martínez-Ros, R. Verdú-Monedero, *IEEE Antennas Wireless Propag. Lett.* **2010**, *9*, 518.

[25] F. Scattone, M. Ettorre, R. Sauleau, N. T. Nguyen, N. J. G. Fonseca, *IEEE Trans. Antennas Propag.* **2015**, *63*, 5854.

[26] J. H. Kim, S. W. Choi, *IEEE Access* **2020**, *8*, 226059.

[27] J. L. Gómez-Tornero, M. Poveda-García, P. Vivo-Vera, R. Verdú-Monedero, in *15th European Conf. on Antennas and Propagation (EuCAP)*, IEEE, Piscataway, NJ **2021**, pp. 1–5.

[28] F. Heidari, Z. Adelpour, A. Mallahzadeh, N. Parhizgar, *AEU - Int. J. Electron. Commun.* **2021**, *135*, 153679.